O and H isotopic evidence for a mantle source of water in appinite magma: an example from the Late Neoproterozoic Greendale Complex, Nova Scotia

Ian P Cawood[a], J Brendan Murphy[b], William J McCarthy[c], Adrian J Boyce[d]

[a]*Department of Earth Sciences, University of Oxford, OX1 3AN, UK*

[b]*Department of Earth Sciences, St Francis Xavier University, NS B2G 2W5, Canada*

[c]*School of Earth and Environmental Sciences, University of St Andrews, KY16 9AL, UK*

[d] *Scottish Universities Environmental Research Centre, G75 0QF, UK*

ABSTRACT

Appinite suite rocks occur as small plutonic bodies, ranging from ultramafic to felsic in composition, that are characterized by abundant idiomorphic amphibole suggesting they are the products of water-rich mafic magmas. Appinites are also understood to record tectono-magmatic processes during the waning stages of subduction in convergent to collisional tectonic settings. Measuring D/H and $^{18}O/^{16}O$ ratios of hornblende in appinitic rocks offers opportunities to constrain the sources of water (mantle, crustal, sea water and or meteoric) in the magma during its crystallization, and to shed light on the role of water as arc magmatism shuts down. The ca. 607 Ma Greendale Complex in the Avalon terrane of Nova Scotia, Canada, is characterized by spectacular exposures of appinite suite rocks ranging from ultramafic to felsic in composition. Two populations of amphiboles are identified: one is characterized by $\delta^{18}O$ values between 4.7–

6.8 ‰ and anomalously low δD values (ca. < -90 ‰). These isotopic signatures are interpreted to represent incorporation of mantle-derived fluids into the crystal structure, possibly associated with mixing between a region of mantle upwelling and a subducting slab. This mixing process allows for hydration of the magma during its ascent into the overlying lithospheric mantle wedge. Some amphiboles retain mantle-like $\delta^{18}O$ and δD values, but others may have partially re-equilibrated during low T assimilation of supracrustal units (e.g. organic-rich sediments) and or fluids derived from such bodies. A second generation of hornblende yields $\delta^{18}O$ varying from 0.9 to 4.6 ‰ and δD from ca. -106 to -64 ‰, which supports equilibration with fluids from crustal sources. Assimilation of volatiles sourced from previously hydrothermally altered intruded sheets and or country rock is interpreted to produce these second-generation isotopic signatures. Regional syntheses indicate that arc magmatism in the Avalon terrane ended with the generation of a transform system, implying the potential generation of a slab window behind that system. In that context, the Appinites in the Avalon terrane have previously been interpreted to have been emplaced after the cessation of subduction in a slab window or slab failure setting behind the transform system, in which asthenospheric upwelling generated juvenile magmas and/or facilitated melting of the overlying continental lithospheric mantle. Our δD and $\delta^{18}O$ data support this model and together with available Sm-Nd data, suggest asthenospheric upwelling triggered melting of the continental lithospheric mantle that was previously hydrated by subduction and this mantle-derived water contributed to the origin of appinites.

1. Introduction

Appinitic suite rocks occur in relatively small plutonic complexes typically around the periphery of voluminous granitoid batholiths (Atherton and Ghani, 2002; Bea et al., 1999; Castro

et al., 2003; Fowler, 1988; Fowler et al., 2001; Murphy, 2013, 2020; Pitcher, 1997; Pitcher and Berger, 1972). They are characterized by abundant idiomorphic amphibole, relative to olivine and pyroxene, in rocks of mafic and ultramafic composition which, together with the widespread development of mafic "pegmatites", indicate that precursor magmas were anomalously water-rich (e.g. Bowes and McArthur, 1976; Murphy, 2013, 2020; Pitcher and Berger, 1972; Pitcher and Hutton, 2003). This interpretation is supported by a plethora of experimental studies which shows that at high pH_2O the stability field of amphibole expands relative to olivine, pyroxene, and plagioclase (Moore and Carmichael, 1998; Müntener et al., 2001). However, the source(s) of this water in appinites has never been directly investigated.

Appinites have a geochemical signature indicative of calc alkaline to shoshonitic affinities (e.g. Atherton and Ghani, 2002; Castro et al., 2003; Fowler, 1988). Their distinctive geochemistry has led to hypotheses postulating genetic relationships with high-Mg basalts (Tiepolo et al., 2011), shoshonitic lamprophyres (Rock, 1990), adakites (Ye et al., 2008), and sanukitoid and tonalite-trondhjemite-granodiorite (TTG) suites (Wilkin and Bornhorst, 1993). Sanukitoids have been postulated as markers of the beginning of post-Archean-style subduction (Fowler and Rollinson, 2012). Many studies also propose a genetic relationship between appinite complexes and granitoid batholiths (e.g. Bowes and McArthur, 1976; Fowler, 1988; Pitcher, 1997). Recent syntheses suggest that appinite suite rocks may preserve evidence of mantle processes that produce voluminous granitoid batholiths (Murphy, 2020) implying that understanding the source of the water from which they crystallize may also constrain models for granitoid magma genesis thus providing insight on the generation of continental crust (Collins et al., 2020).

Appinites are spatially associated with deep crustal faults and geodynamic processes associated with the cessation of subduction, such as post-subduction slab-break off, slab window generation and slab delamination during the latest stages of an orogeny (Atherton and Ghani, 2002; Castro et al., 2003; Murphy, 2013, 2020; Murphy and Hynes, 1990; Ye et al., 2008). Given the important role of water genesis in the production of arc magmas, the origin of water in appinite complexes has the potential to shed light on processes operating as subduction shuts down.

In this study, we focus on the late Neoproterozoic Greendale Complex, a spectacularly exposed body of appinite suite rocks in the Avalon terrane of northern Nova Scotia. We provide oxygen and hydrogen isotopic data on hornblende in various lithologies in this complex to constrain the sources of the water that resulted in hornblende crystallization. Our data identify an important component of mantle-derived water, which has implications for the origin of magmas in the waning stages of arc magmatism.

2. Geological setting and field relationships

The late Neoproterozoic (607 ± 2 Ma, U-Pb titanite) Greendale Complex is a local representative of subduction-related magmatism that characterizes the Avalon terrane in the Canadian Appalachians (Murphy et al., 1997a). This magmatic activity occurred when Avalonia was located along the northern Gondwanan margin prior to its Late Cambrian-Early Ordovician separation from Gondwana and Late Silurian-Early Devonian accretion to Laurentia (Fig. 1a; Murphy et al., 1997b). The Greendale Complex occurs between two faults, the Hollow and

Greendale faults, which were active at the time of its emplacement (Fig. 1b, c; Murphy and Hynes, 1990). The complex intrudes the Chisholm Brook Formation (dominated by basalt with minor limestone) and the Morar Brook Formation (dominated black organic mudstone and siltstone, with minor limestone and chert) of the late Neoproterozoic Georgeville Group, a polydeformed arc-related sequence largely composed of greenschist facies volcanic and sedimentary rocks (Murphy et al., 1990). A maximum depositional age of 613 ± 5 Ma (U-Pb, detrital zircon; Keppie et al., 1998) implies limited time between deposition, deformation and metamorphism of the Georgeville Group rocks and intrusion of the Greendale Complex. Intrusion of the complex is coeval with larger 615–605 Ma granitoid intrusions in the central and southern Antigonish Highlands and two smaller (and poorly exposed) appinite bodies in the southernmost highlands (Keppie et al., 1990; White et al., 2021). These relationships imply that the Greendale Complex has a similar peripheral location with respect to coeval granitoid bodies to that documented in the type area for appinites in the Scottish Caledonides. The emplacement of the Greendale Complex is interpreted to be broadly synchronous with regional strike-slip activity, which occurred after cessation of subduction (Murphy and Hynes, 1990).

The Greendale Complex consists of steeply dipping intrusive sheets ranging from ultramafic to felsic in composition thought to have been emplaced by multiple and repeated injections of compositionally diverse magma. Orientations of igneous layers within the complex are consistent with emplacement along extensional fractures during dextral shear along the Greendale and Hollow faults (Murphy and Hynes, 1990). Though the complex is largely dominated by hornblende-rich medium grained to porphyritic gabbro, abundant heterogeneity is observed at all scales with obvious mixing and mingling between units (Fig. 2a, b; Murphy et al., 1997b).

Lithologies vary in grain size from fine grained “salt and pepper” texture to pegmatite with euhedral amphibole crystals up to 15 cm in length (Fig. 2a, c, d). The pegmatitic amphiboles commonly enclose plagioclase cores and appear acicular and skeletal – these textures are attributed to rapid growth from a water-rich magma (Murphy et al., 2012). Internal contacts between intrusive units vary from sharp to gradational, planar to irregular and scalloped (Fig. 2a, b). These contacts commonly show varying degrees of assimilation and disintegration resulting in locally hybrid intermediate rocks characterized by trains of autoliths and autocrysts (Murphy et al., 1997b). Xenoliths of the host rock Morar Brook and Chisholm Brook Formation are also common, especially adjacent to external contacts.

A study of crystal-chemical parameters of white micas in Georgeville Group host rocks from the aureole of the Greendale Complex indicates emplacement at pressures of no more than 3–5 kbar (Abad et al., 2011). The Al content in hornblende (see Anderson and Smith, 1995; Putirka, 2016) supports hornblende crystallization at 5–7 kbar at temperatures between 650–750 °C (Pe-Piper and Piper, 2018).

3. Petrography and geochemistry

3.1 Mineralogy and textures

The mineralogy and main textural features of the Greendale Complex are described in detail in Murphy et al. (2012) and are summarized below, further details are added where relevant. Amphibole is the overwhelmingly dominant mafic mineral in both the mafic and ultramafic rocks.

Ultramafic rocks account for 5–10 % of exposed lithologies and are dominated by hornblende, pyroxene and olivine and are classified as hornblende peridotites, pyroxene hornblendites or olivine–pyroxene hornblendites (Murphy et al., 2012; 'corlandtites' e.g. Bea et al., 1999). Olivine occurs as medium grained (0.1–3.5 mm) rounded hypidiomorphic chadacrysts hosted within hornblende and or clinopyroxene. The olivine ranges from Fo_{86} to Fo_{75}, contains inclusions of chromite and is variably altered to talc or serpentine (Fig. 3a). Pyroxene (dominantly clinopyroxene) occurs as xenomorphic to hypidiomorphic chadacrysts (0.5–6 mm) within hornblende. Clinopyroxene includes endiopside, augite and sub-calcic augite with Mg# ranging from 0.62 to 0.79. Rare orthopyroxene (hypersthene) has Mg# between 0.85 and 0.86 and very low Ca (> 0.05). Hornblende appears as two populations: 1) large (1.0–8.0 mm) hypidiomorphic oikocrysts enclosing clinopyroxene and olivine, defining a poikilitic texture (Fig. 3b, c) and 2) modally minor grains (0.5–5.0 mm), that are interstitial with plagioclase, phlogopite, and opaques. In most samples, plagioclase ranges from $An_{50–60}$; rare grains with An_{75} occur.

Mafic rocks are dominantly defined by the presence of plagioclase and hornblende. Plagioclase appears as hypidiomorphic to idiomorphic tabular grains of variable size (ca. 0.2–1.0 mm). It is typically extensively saussuritised, though euhedral forms are preserved as stubby lath-shaped crystals (Fig. 3d). Plagioclase may also have fresh irregular albitic rims that surround saussuritised cores (Fig. 3e). Interlocking grains are dominantly found in the phaneritic matrix. Plagioclase shows regular polysynthetic twinning and is typically labradorite in composition (An_{60}–An_{65}) with normal to oscillatory zoning also occurring (ranging from An_{40}– An_{65}). Hornblende occurs in mafic rocks as hypidiomorphic prismatic to acicular grains (0.5–7.0 mm)

150 that may contain inclusions of plagioclase and boundaries that are commonly impinged by
151 plagioclase laths. Plagioclase inclusions contain both saussuritised cores and albitic rims which
152 implies that this feature likely results from chemical zonation (e.g. Ca-rich core) rather than
153 sequential growth events. Taken together, these textures indicate hornblende and plagioclase
154 were co-precipitating liquidus phases (Fig. 3d, f).
155
156 Felsic rocks make up 5–10 % of the Greendale Complex and occur as discrete sheets,
157 isolated pods and segregations within relatively mafic lithologies. They range from aplite to
158 pegmatite in texture and rhyodacite to rhyolite in chemical composition. Hornblende is less
159 abundant than in the mafic rocks and is observed as xenomorphic grains (ca. 0.5–2.0 mm)
160 commonly pseudomorphed by chlorite and/or actinolite. Plagioclase is the dominant matrix
161 phase and occurs as an interlocking network of heavily saussuritised tabular grains (0.5–3.0
162 mm). Inclusions of plagioclase within hornblende show lesser degrees of saussuritisation.
163
164 These petrographic observations suggest that two populations of hornblende occur in the
165 suite of rocks studied. One population, dominant in ultramafic rocks, displays oikocrysts of
166 hornblende enclosing chadacrysts of olivine and pyroxene. The other population, dominant in the
167 mafic and felsic rocks, exhibits impinged grain boundaries and/or inclusions of plagioclase.
168
169 **3.2 Geochemistry**
170 Previously published mineral geochemical data for amphiboles in mafic and ultramafic
171 samples and lithogeochemical data for representative rock specimens (Murphy et al., 1997b;
172 Murphy et al., 2012), are summarized here. Amphibole compositional data from felsic rocks was

not collected by previous studies. All amphiboles are calcic according to the classification of Leake et al. (2004) and their compositions are typical of igneous amphiboles. Classification is based on the following general chemical formula:

$$A_{0-1}B_2C^{VI}{}_5T^{IV}{}_8O_{22}(OH,F,Cl)_2$$

A plot of four-fold Al (Al^{IV}, T site) vs total Al (Al^{tot}) data from amphiboles of ultramafic and mafic rocks (Fig. 4) shows that Al resides in both Al^{IV}, T and Al^{VI}, C sites but appears to have a preference for the tetrahedral site, consistent with the interpretation that edenite substitution ($Na,K^A+Al^{IV}=Si^{IV}$) dominates over tschermak ($Al^{IV} + Al^{VI} = Si^{IV} + (Fe, Mg)^{VI}$ substitution (Murphy et al., 2012).

Amphiboles from ultramafic rocks are also dominated by magnesio-hornblende with low SiO_2 (44.3–52.1 wt.%) and Al_2O_3 (6.2–11.9 wt.%) and high MgO (13.4–23.9 wt.%) and high Fe_2O_3 (8.6–12.8 wt.%). A small amount of variation is observed in Mg# (0.71–0.79). Two groupings of amphiboles are distinguished on the basis of REE abundances. Group A amphiboles display a slight LREE enrichment, small negative Eu anomaly, minor decrease in HREE and significant enrichment in LILE. Group B amphiboles display enrichment in LREEs, depletion in HFSEs and HREEs and lack a negative Eu anomaly (Fig. 5). Lithogeochemical analyses of ultramafic rocks are characterized by a depletion in HFSE and high abundances of MgO (13.4–23.9 wt.%), Cr (462–2146 ppm), Ni (54–510 ppm) and Ba (< 5–246 ppm).

Amphiboles from mafic rocks are tschermakite, tschemakitic hornblende, and magnesio-hornblende in composition (Murphy et al., 2012). Amphiboles from mafic rocks have a significantly lower Mg# (0.31–0.48) than the ultramafic rocks (0.71–0.79) though amphiboles

196 from both rock types share a remarkably uniform Mg# over a range in Si (up to one formula
197 unit). REE profiles are characterized by depletion in LREE (La/Sm≈0.61), a slight depletion in
198 HREE (Gd/Yb≈1.55) as well as a negative Eu anomaly, which is interpreted to reflect co-
199 precipitation of plagioclase (Group A). Compared to ultramafic rocks, lithogeochemical analyses
200 of mafic samples have a limited range in SiO_2 (45.8–52.08 wt.%), a higher Al_2O_3 (17.3–19.6
201 wt%), slightly lower Fe_2O_3 (7.6–11.5 wt.%), and substantially lower MgO (4.0–8.6 wt.%), Ni
202 (<5–31ppm) and Cr (11–200 ppm). Although REE and HFSE patterns for mafic rocks have
203 broadly similar profiles to the ultramafic rocks, depletion of HFSE (e.g. Nb, Zr and Ti) isn't as
204 strong and they also record a pronounced negative Eu anomaly.
205
206 Intermediate to felsic rock samples have wide ranges in SiO_2 (58.0–80.8 wt.%) and Al_2O_3
207 (10.7–22.9 wt.%), but relatively low MgO (0.6–1.6 wt.%), V (6–59 ppm), and Cr (25–47 ppm).
208 They have similar Mg# (0.33–0.48) to the mafic samples, are weakly depleted in HSFE and
209 exhibit a pronounced negative Eu anomaly. Whole rock Sm-Nd data (Murphy and Dostal, 2007)
210 imply an origin by crustal anataxis. Field and geochemical evidence indicate that most of the
211 intermediate rocks formed from mixing and mingling of mafic and felsic end members (Fig. 2a).
212
213 Amphibole groups A and B (defined by contrasting REE and normalized trace element
214 profiles) are interpreted to be coincident with the two petrographic populations outlined in the
215 previous section (Group A = coprecipitation of hornblende and plagioclase, Group B =
216 hornblende poikilitically enclosing olivine and clinopyroxene). As such these "geochemical
217 groups" and "petrographic populations" will be referred to exclusively as Group A and Group B

herein. In the following discussion, groups A and B will be placed in context of their δD and $\delta^{18}O$ isotopic characteristics.

4. Methods

Magma systems may incorporate volatiles of several components and phases, though given the textures and amphibole rich mineralogy of the appinite suite, such features indicate that water acts as the dominant component (e.g. Murphy et al., 2012). As such, we will be focusing on the behavior of water in magmatic systems.

Individual amphibole grains were separated from hand specimens using either a Dremel microdrill or picked under binocular microscope following light crushing of specimens. Drilled samples were collected by excavating ca. 1–2 mm into fresh hornblende grains. Hand-picked grains were sonicated in distilled water to remove associated micas and powder from crushing. Fresh hornblende grains with few inclusions, and minimal or no alteration were preferentially selected to reduce contamination and the effects of late-stage alteration on analysis. For felsic samples, where late-stage alteration is widespread, grains with the least amount of alteration were selected. Petrographic observations were key in constraining the degree of alteration present in the thin sections and thus informed where rock specimens were inappropriate for sampling. Given that the methodology for isotopic analysis removes drilled or crushed/picked grains from a cut-off rather than a thin section (where textural relationships are clear), petrographic observations simply provided useful context for the degree of alteration within a given specimen number.

241 Oxygen was extracted from amphibole separates (ca. 0.1–0.2 mg) via silicate fluorination
242 with excess ClF_3 following the method of (Sharp, 1990). Overnight pre-fluorination at room
243 temperature removes unbound water. Fluorination with a CO_2 laser at temperatures in excess of
244 1500 ºC results in total sample reaction and release of O_2 from the mineral lattice. The O_2 is
245 converted to CO_2 by reaction with hot graphite and analyzed on a VG SIRA II mass
246 spectrometer. $\delta^{18}O$ values reported as per mil (‰) deviations from Vienna Standard Mean Ocean
247 Water (V-SMOW). Mineral separates for hydrogen isotopic analysis (ca. 40 mg) were degassed
248 overnight (150 ºC). Hydrogen was extracted by *in vacuo* bulk heating using the method of
249 Donnelly et al. (2001). Water was reduced using a chromium powder furnace (830 ºC) and
250 resulting H_2 (from the OH site) analyzed on a VG Optima mass spectrometer. δD values are
251 reported as per mil (‰) deviations from V-SMOW. The yield (%) from hydrogen isotope
252 analysis was used to estimate the water content (wt. %) of each sample. Water content estimates
253 for samples should be considered as minimum estimates only as amphiboles contained variable
254 amounts of pyroxene, olivine and feldspar inclusions in some cases. Reproducibility of O isotope
255 data, based on repeat analyses of international and internal lab standards, was typically better
256 than ± 0.3 ‰, with standards averaging as follows: garnet UWG-2 = 5.7 (U Wisconsin
257 international garnet standard with accepted value = 5.8 ‰); YP-2 = 16.4 ‰ (internal quartz
258 standard should be 16.4 ‰); SCXO = 5.2 ‰ (San Carlos olivine standard should be 5.2 ‰).
259 Reproducibility of hydrogen isotope analyses of pure water secondary standards was better than
260 ± 2 ‰ around the time of these analyses, with standards averaging as follows: seawater = -5 ‰
261 (versus accepted value of -6); Lt Std = -93 ‰ and -95 ‰ (versus accepted of -94 ‰); and GISP
262 = -188 ‰ (versus accepted = -189 ‰).
263

5. Results

5.1 O and H isotopic variation

Measured $\delta^{18}O$ and δD values are presented in Tables 1 and 2. The $\delta^{18}O$ values shown in Figure 6 and Table 1, range between 0.9 ‰ and 6.8 ‰ with the lowest values recorded in the amphiboles from felsic rocks and highest values recorded in the amphiboles from ultramafic rocks. Individual ultramafic rock samples have amphibole $\delta^{18}O$ sample averages ranging from 4.9 to 6.2 ‰ with all ultramafic samples producing a rock type average of 5.7 ‰. Amphiboles from mafic rocks have $\delta^{18}O$ individual rock sample averages ranging from 3.6 to 5.2 ‰ with all mafic samples averaging 4.4 ‰. Amphiboles from felsic rocks have $\delta^{18}O$ individual rock sample averages ranging from 2.1 to 3.1 ‰ with an overall rock type average of 2.6 ‰. Large variations are recorded within δD measured across the samples. Amphibole δD values range between -135 ‰ and -64 ‰ (Table 2, Fig. 7) with the highest values recorded in the amphiboles from felsic rocks (-68 to -64 ‰, average -66 ‰), moderate values in the amphiboles from mafic rocks (-106 to -88 ‰, average -99 ‰) and lowest (most D depleted) values in the amphiboles from ultramafic rocks (-135 to -88 ‰, average -103 ‰). Only sample GR5-F contained enough amphibole for H isotopic analysis from the felsic units – though there was enough to run twice. Thus, we take the value to be representative of amphiboles taken from felsic rocks as only 4 ‰ deviation is recorded between the two measurements.

5.2 Fractionation of fluid phase

Calculating the composition of a fluid phase that has been removed from the original mineral-fluid system requires knowledge of isotopic fractionation factors between hydrous minerals and fluid. Fractionation factors are influenced by temperature, pressure, fluid

composition and mineral composition (Chacko et al., 2001). Most fractionation factors are derived from experimentally determined mineral-mineral fractionations as summarized in Chacko et al. (2001) and Valley (2003). However, as no experimental data are available for O isotopic fractionation in amphiboles, estimates of fractionation are based on theoretical predictions (Zheng, 1993). Although this practice is inferior to experimentally derived fractionation, until further studies have been completed, we are implementing the best available values. Difficulty arises with amphibole-water H isotope fractionations given by Suzuoki and Epstein (1976) and Graham et al. (1984), which show differences related to the effects of Fe on mineral-water fractionations. Some of the differences are likely due to differences in pressures used during their experiments, however the reason for this is not fully understood (Chacko et al., 2001; Marks et al., 2004). No clear inverse relationship is visible between measured δD and $Fe_{(tot)}$ as would be expected by Suzuoki and Epstein (1976; Fig. 8a), though given potential errors involved in estimations of Fe^{3+}/Fe^{2+} ratios from electron microprobe analysis (e.g. Feldstein et al., 1997) we do not take this to favour one set of calculations over the other.

The measured $\delta^{18}O$ and δD of the amphiboles can be used to calculate the isotopic composition of the fluid phase the amphiboles precipitate from. Amphibole-water oxygen isotope fractionation at a temperature average of 700 °C is -2.3 ‰ (expressed as $1000ln_{\alpha\ amph-water}$) according to the equations of Zheng (1993). This produces a $\delta^{18}O$ fluid isotopic composition of 3.1 to 9.1 ‰ (see Table 1). Amphibole-water hydrogen isotope fractionations at 700 °C can be as large as -32 ‰ (Graham et al., 1984) or as low as -17 ‰ (Suzuoki and Epstein, 1976). This produces a fluid phase composition of -118 to -47 ‰ for the calculations of Graham et al. (1984) and -103 to -32 ‰ for the calculations of Suzuoki and

Epstein (1976; see Table 2). Calculated fluid $\delta^{18}O$ and δD are plotted against each other in Figure 9a, b.

6. Discussion

6.1 Pressure-Temperature constraints

The calculation of pressure-temperature (P-T) conditions in igneous rocks may be used to estimate the depth of magma crystallization and/or emplacement. When compared to mineral and fluid isotope signatures, these two data sources may be used to derive if a given mineral precipitated at the fluid source or away from it (e.g. Ulrych et al., 2018). The Greendale Complex is interpreted to have been emplaced at shallow structural levels during dextral motion along strike-slip faults (Murphy and Hynes, 1990). The abundance of pegmatitic hornblende gabbro, widespread roof pendants, and miarolitic cavity textures indicate the Greendale Complex is exposed near the pluton roof (Murphy et al., 2012).

Both Group A and Group B amphiboles are igneous in composition and their geochemistry is sensitive to changes in pressure and temperature as well as magma composition. A variety of amphibole-based thermobarometers have been proposed to estimate P-T conditions of crystallization for different igneous systems (e.g. Putirka, 2016; Ridolfi and Renzulli, 2012). Although the thermobarometer of Ridolfi and Renzulli (2012) is suitable for the host rock composition, we deem it unsuitable for the purposes of this study as its sensitivity to compositional variations in amphibole may introduce large uncertainties in estimations of crystallization conditions (Ulrych et al., 2018). Although the Al content of hornblende indicates crystallization at 5–7 kbar and between 650–750 °C (Anderson and Smith, 1995; Pe-Piper and

Piper, 2018), Figure 10a suggests that temperature conditions could have been closer to 650 °C which supports crystallization between 5–8 kbar. The empirical barometer of Pál-Molnár et al. (2015), calibrated using the Al_2O_3 contents of experimentally produced amphiboles, suggests crystallization pressures concentrated between 6.7–9.0 kbar, though significant variation of pressure is observed across Al_2O_3 contents. Results using calculations in Pe-Piper and Piper (2018) are thus preferred. Comparing the Al_2O_3 contents of Greendale Complex amphiboles against the calculations of Anderson and Smith (1995) shows crystallization predominantly occurred between 7–8 kbar at or near to 650 °C (Fig. 10b). Given the emplacement depth is likely between 3–5 kbar (Abad et al., 2011), it appears that a significant proportion of hornblende growth occurred at deeper structural levels, but was transported upwards by ascending magma.

6.2 Oxygen isotopes

Oxygen is the most abundant element in ordinary rocks, making up approximately 50 wt. %, thus silicate oxygen has a major influence on the observed $\delta^{18}O$ for the water-to-rock ratios that likely exist in these systems. The $\delta^{18}O$ of a mineral and the related fluid from which it crystallizes or re-equilibrates with, may be determined by the exchange of oxygen between the mineral and fluid, and the temperature at which this exchange occurs (Sheppard, 1986a). Equilibrium $\delta^{18}O$ values of igneous minerals decrease as follows: quartz > alkali-feldspar > calcic plagioclase > biotite > apatite > orthopyroxene > zircon > clinopyroxene > amphibole > garnet > olivine > oxides (Eiler, 2001; Valley, 2003). Minerals such as olivine, magnetite and amphibole typically have lower $\delta^{18}O$ values than basaltic melts at magmatic temperatures and so precipitation of these minerals increases $\delta^{18}O$ in the residual melt. However, crystallization and fractionation of quartz or albitic plagioclase or K-feldspar from a melt deplete the residual melt

356 in ^{18}O (Bucholz et al., 2017). Relicts of clinopyroxene and olivine, which are the most significant
357 inclusions in amphibole samples, have a limited effect on the range in $\delta^{18}O$ values because
358 pyroxene and olivine fractionation have a similar effect to amphibole (Zheng, 1993). Study of
359 variations in oxygen isotopic composition in magmas during fractional crystallization indicate
360 that higher temperature systems should experience limited increases in $\delta^{18}O$ (Taylor, 1968).
361
362 The sampling method for isotopic analysis removes grains from their textural
363 relationships, therefore it is not possible to directly correlate isotopic results with groups A and B
364 as defined by their REE profiles, trace element abundances and petrographic observations.
365 However, there are two distinct isotopic signatures (e.g. Fig. 6), which trace the origin and depth
366 of fluids from which the two amphibole populations precipitate. We interpret these two distinct
367 isotopic signatures to likely represent the same processes acting to form the two petrographic and
368 geochemical populations previously described.
369
370 *Group B amphibole*: In general, minerals crystallizing in equilibrium with mantle-derived
371 magmas and fluids typically exhibit a restricted O isotopic range of 5.3 ± 0.6 ‰ (Valley et al.,
372 1998) or 5.3–5.6 ‰ (amphibole, Chazot et al., 1997) or 5.5 ± 0.2 ‰ (MORB, Bindeman, 2008).
373 The first two studies imply that Group B amphiboles in both ultramafic samples (4.0–6.8 ‰) and
374 mafic samples (2.5–5.3 ‰) have predominantly mantle-derived water (which is supported by
375 petrographic observations where mafic and ultramafic samples both contain Group B
376 amphiboles). Whereas the final study implies only ultramafic Group B amphiboles contain
377 mantle-derived water (Fig. 6). Geochemical analyses show depletion of ultramafic rocks in
378 HFSE and high abundances of MgO, Cr, Ni and Ba. These geochemical signatures support a

mantle fluid source in a subduction zone setting (Atherton and Ghani, 2002; Pearce, 1983). Elevated O isotopic values (> 5.9 ‰), as seen in Figure 6, are typically attributed to low T melting or assimilation of supracrustal sedimentary or volcanic rocks (Valley et al., 2005).

The range in Group B amphibole values (ca. 4.7–6.8 ‰) suggests that the water was largely mantle-derived. Given that the amphiboles likely crystallized at depths equivalent to 5–8 kbar, these data imply that this water was dissolved in mantle-derived magma and ascended to a depth of ca. 12–16 km whereupon Group B amphiboles began to crystallize. This scenario is broadly consistent with that depicted by Collins et al. (2020) in which subduction generates hydrous basaltic magmas in the overlying mantle wedge that exsolve water as they cool beneath the Moho.

Some amphiboles retained mantle-like $\delta^{18}O$ values, whereas others with high $\delta^{18}O$ may have partially re-equilibrated during low T water-rock interactions in supracrustal conditions. This is similar to the manner described by Pitcher (1997), olivine-pyroxene-hornblende textural relationships in appinites are interpreted to result from the upward transport and hydration of olivine-pyroxene cumulates in water-rich mafic magma. These cumulates reacted to form amphibole during ascent. Group B amphiboles in mafic and ultramafic rocks display a poikiloblastic texture of oikocrysts of hornblende enclosing chadacrysts of olivine and pyroxene. Textural relations support the sequence of timing suggested by Pitcher (1997), however, olivine and pyroxene did not react to form hornblende (Fig. 3b, c).

401 *Group A amphibole:* The lower $\delta^{18}O$ values (< 4.7 ‰) of Group A amphiboles indicate their
402 fluid source was contaminated by high-T hydrothermal cycling of meteoric water into shallow
403 (epizonal) magma systems before or during crystallization (Bindeman, 2008). Petrographic
404 observations show extensive saussuritisation of plagioclase and pseudomorphing of hornblende
405 by chlorite and/or actinolite, supporting availability of excess fluids during and/or after
406 crystallization. Field evidence for extensive mixing and mingling between intrusive phases
407 (Murphy et al., 1997b) suggests that the water source for some Group A amphiboles may have
408 come from earlier hydrothermally altered appinite sheets (see Valley, 2003; Valley et al., 2005).
409 According to Boroughs et al. (2012), direct interaction of crystallizing magma and meteoric
410 water is improbable because 1) meteoric-hydrothermal systems commonly reside at significantly
411 lower pressures than magmatic systems, and 2) magmas cannot ingest enough fluid to produce
412 very low $\delta^{18}O$ magma. Studies have shown that assimilated hydrothermally altered country rock
413 can produce relatively small shifts (< 2 ‰) in $\delta^{18}O$ (Wolff et al., 2002). Thus, water
414 accompanying crystallization of Group A amphiboles was possibly sourced from previously
415 intruded hydrothermally altered sheets.
416
417 Oxygen isotope exchange between hornblende and feldspar at decreasing temperatures
418 may also result in a negative $\delta^{18}O$ shift (Demény et al., 2008). Hornblende oxygen-self-diffusion
419 closure temperatures are around 600–800 °C (at 100–1000 °C Ma^{-1} cooling rate and 0.1–1.0 mm
420 grain size; Farver, 1989). These temperatures are broadly compatible with crystallization
421 temperatures for hornblende of the Greendale Complex (650–750 °C; Pe-Piper & Piper, 2018),
422 implying that oxygen isotope exchange between hornblende and feldspar was only possible

during crystallization of the hornblende, therefore unlikely to solely responsible for the negative $\delta^{18}O$ shift.

The calculated composition of the fluid $\delta^{18}O$ from which the amphiboles crystallized ranges from 3.1 to 9.1 ‰. The spread of these values support heterogeneity in the amphibole water source.

6.3 Hydrogen isotopes

Hydrogen is usually a trace element in rocks (ca. < 2000 ppm), a rock with 1 wt. % H_2O contains approximately 0.11 wt % hydrogen. In contrast to oxygen (ca. 50 wt. %), this means the hydrogen budget is more strongly influenced by the interacting fluid (Sheppard, 1986a). Due to limited fractionation of δD between amphiboles and mantle fluids (-80 ± 5 ‰ from pristine MORB glasses, Kyser and O'Neil, 1984), δD variations in amphiboles and associated fluids from which they crystallize may be interpreted to reflect mantle heterogeneities and/or the influence of crustal contamination and metasomatic fluids within mantle-derived rocks. Amphiboles analyzed in this study have highly D-depleted isotopic compositions (δD = -135 ‰ to -64 ‰) when compared to the normal range for mantle amphiboles (ca. δD = -100 to -20 ‰; Hoefs, 2018 and references therein). Various explanations have been proposed to explain low δD amphibole values in magmatic rocks:

1. *Oxidation of Fe^{2+} to Fe^{3+} in magmas.* This causes degassing of molecular H_2 (Mathez, 1984; Sato, 1978), which can result in enrichment in D in the residual phases (e.g. Kyser 1986) via reaction (1).

$$2Fe^{2+}_{(melt)} + 2H_2O \rightarrow 2Fe^{3+}_{(melt)} + 2OH^- + H_2 \qquad (1)$$

Released molecular hydrogen is typically depleted in deuterium relative to water. Thus, if amphibole crystallizes at increasingly oxidizing conditions with significant degassing, there should be a resulting increase in the δD of amphibole with increasing Fe^{3+}/Fe^{2+} ratios (Kyser, 1986; Marks et al., 2004). However, the variations in δD show a weak inverse correlation with Fe^{3+}/Fe^{2+} (Fig. 8b), suggesting that variations in oxidation state of the magma cannot account for the low values or the range in amphibole δD.

2. *Major degassing of magmatic water*. Experimental studies by Kuroda et al. (1982) and Dobson et al. (1989) show that water exsolved from a melt may be enriched (+20 to +50 ‰) in δD relative to the remaining melt. Exsolved water ascends and percolates to upper parts of the magma system (Agemar et al., 1999; Collins et al., 2020). According to Rayleigh-type models, degassing should be characterized by a correlation of exponentially decreasing δD values and decreasing water content in magmatic rocks or constituent minerals (Marks et al., 2004; Taylor et al., 1983). In our data set however, on average, the lowest δD values are more typically derived from the less fractionated ultramafic-mafic samples that dominantly contain Group B amphibole, which are less evolved than Group A amphibole (Murphy et al., 2012), which is inconsistent with the degassing trend (Fig. 11a, b). Furthermore, the extreme water loss required to acquire the low δD values would destabilize formation of late amphibole (Marks et al., 2004). Magmatic degassing is thus not regarded as a viable process to explain the low δD values.
3. *Input of volatiles from recycled oceanic lithosphere*. Mixing between a water-rich high δD subduction-related component and a separate component characterized by water-poor and low δD has been proposed as a possible explanation for linear trends between H_2O

(wt. %) and δD (Shaw et al., 2008, 2012). Experimentally determined fractionation factors between hydrous minerals and water indicate that fluid released from a dehydrating subducting slab, should be D-enriched (Graham et al., 1984; Suzuoki and Epstein, 1976; Vennemann and O'Neil, 1996). Consequently, recycled oceanic lithosphere is predicted to yield a low δD water component as the progressively dehydrated slab releases D-enriched fluids into the overlying mantle wedge (Shaw et al., 2008). Given the field evidence for extensive mingling between intrusive phases (Murphy et al., 1997b), this process is unlikely to be solely responsible for the δD isotopic signature, however it explains the linear trend of amphibole δD values with water content and is thus interpreted to be a dominant source of fluids for ultramafic-mafic samples of Group B amphiboles (ca. < -100 ‰; outside the normal mantle amphibole range provided in Hoefs, 2018 and references therein).

4. *Influx of hydrothermal-meteoric fluids during crystallization* (e.g. Agemar et al., 1999). This process is consistent with the abundance of low $\delta^{18}O$ values (< 4.7 ‰) found dominantly within mafic and felsic amphiboles (Group A), which support a fluid source from previously intruded hydrothermally altered sheets. This process could thus explain some of the δD signatures found within some felsic and mafic rocks (δD -106 to -64 ‰). However, it does not explain the anomalously low δD values abundant in the ultramafic rocks, which dominantly contain Group B amphiboles from petrographic observations and have mantle-like $\delta^{18}O$ values.
5. *Fluid input derived from organic matter and/or assimilation of organic-rich sedimentary rocks* (e.g. Sheppard, 1986b). The Hollow Fault (Fig. 1c) was active during magma emplacement and directed fluid and magma migration, mixing and mingling from various

sources and crustal levels (Murphy and Hynes, 1990). Assimilation of organic-rich sediments such as those of the Morar Brook Formation or fluid derived from such sediments can explain why a portion of δD and $\delta^{18}O$ fluid values do not plot in the magmatic H_2O field, and instead lie within the organic waters field (δD ca. < -90 ‰; Fig. 9a, b). This process is consistent with high $\delta^{18}O$ values (> 5.9 ‰) related to low T supracrustal contamination for Group B amphiboles (Valley et al., 2005).

Amphibole-water δD isotope fractionations at 700 °C can be as large as -32 ‰ (Graham et al., 1984) or as low as -17 ‰ (Suzuoki and Epstein, 1976). However, the range in values is much smaller than the observed variations in δD and given the poor correlation to amphibole Fe-content, neither can explain the range of values measured. Thus, the data supports heterogeneity in the δD isotopic composition of the source fluid rather than fractionation from it.

6.4 Summary and implications

Appinites may, in principle, form in any tectonic environment in which mafic magmas become anomalously water-rich. However, geochemical, geochronological and field studies indicate appinite complexes are preferentially emplaced after the cessation of subduction (Atherton and Ghani, 2002; Murphy, 2013, 2020 and references therein). In the aftermath of continent-continent collision, such as in the Variscan belt of continental Europe, appinitic magma may be generated by decompression melting (e.g. Castro et al., 2003). The Greendale Complex, however, is one of several late Neoproterozoic appinite complexes documented in Avalonia and Cadomia, two neighboring terranes located along the northern Gondwanan margin at that time. Regional syntheses indicate that in each region, these complexes were emplaced at

514 the termination of arc magmatism, which is interpreted to reflect ridge-trench collision and the
515 diachronous propagation of a San Andreas-style transform fault along the length of the northern
516 Gondwanan margin (Murphy and Nance, 1989). Such an environment generates a slab window
517 setting on the landward side of the transform fault that enables asthenospheric upwelling and the
518 generation of mafic magmas (Fig. 12; e.g. Johnston and Thorkelson, 1997; Sisson et al., 2003).
519
520 Upwelling asthenosphere advects heat into an overlying continental lithospheric mantle
521 previously metasomatised by subduction-derived fluids and underplating hydrous mafic magmas.
522 Experimental evidence indicating that much of this water is stored in calcic amphiboles (such as
523 pargasite) is supported by the widespread occurrence of pargasite in xenoliths from several
524 supra-subduction zone localities (Corgne et al., 2018 and references therein). In the case of the
525 Greendale Complex, asthenospheric upwelling induced melting of a previously hydrated
526 continental lithospheric mantle. This scenario is consistent with Sm-Nd isotopic values of mafic
527 rocks in the Greendale Complex, which are significantly lower than the contemporary depleted
528 mantle and lie within the Avalonian envelope for the Neoproterozoic-Paleozoic evolution of its
529 lithospheric mantle (Murphy et al., 1997b; Murphy and Dostal, 2007). Melting of this hydrated
530 mantle formed a fluid-rich mafic (appinitic) magma. The high $\delta^{18}O$ values of Group B
531 amphiboles (between 4.7–5.9 ‰) reflect incorporation of mantle-derived fluids into the crystal
532 structure. These mantle-derived fluids were initially extracted from the vicinity of a dehydrated
533 (D-depleted) subducting slab producing anomalously low δD values (ca. < -100 ‰) and
534 contaminated the overlying lithospheric mantle wedge either directly (as fluids) or indirectly as
535 hydrous magma which exsolved water as it cooled beneath the Moho (e.g. Collins et al., 2020).
536 This water then became incorporated into appinitic magmas when heat was advected into the

continental lithospheric mantle by asthenospheric upwelling, resulting in progressively D-enriched signatures as supported by the linear trend between δD and water contents (wt. %). Hornblende compositions (Murphy et al., 2012; Pe-Piper and Piper, 2018) indicate equilibration between 3–7 kbar suggesting that mantle water dissolved in the magma and became incorporated into the hornblende structure as the magma rose through the crust by exploiting the Hollow-Greendale fault system. Textures indicative of high growth rate (Murphy and Hynes, 1990) are consistent with rapid ascent of magma as it exploited this fault system.

As the magma migrated further upwards in the crust, it was contaminated by assimilation of organic-rich host rock (which provided a fluid source for supracrustal Group B amphiboles, $\delta^{18}O > 5.9$ ‰, some δD signatures < -90 ‰) and/or by previously hydrothermally altered bodies (dominant fluid source for Group A amphiboles, $\delta^{18}O < 4.7$ ‰, δD ca. -106 to -64 ‰). Overlap between isotopic signatures emphasizes that these processes are not mutually exclusive and that fluid interaction in subduction zones represents a dynamic system. The Hollow-Greendale fault system likely facilitated assimilation into the magma of 1) fluids derived from previously hydrothermally altered bodies, and 2) supracrustal rocks and associated fluids from organic sediments at low T. Felsic δD values are significantly higher and show extensive $\delta^{18}O$ variation when compared to amphibole isotopic signatures from mafic and ultramafic rocks. The late-stage intrusion history of felsic magmas and their extensive alteration implies they likely formed separately to the ultramafic and mafic magmas. This interpretation is compatible with field evidence of extensive mingling between intrusive phases (Murphy et al., 1997b).

Acknowledgments

This project was initiated when IPC was in receipt of a Laidlaw scholarship at the University of St Andrews and was made possible by grant funding from the Geological Society of London (Joseph Burr Tyrrell Fund) and by NSERC, Canada (2020-03872). The authors are thankful to the analytical scientists at SUERC, UK for their time and patience spent aiding in collection of the isotopic data. Constructive and insightful comments from Mike Fowler and Antonio Castro greatly improved this manuscript.

References

Abad, I., Murphy, J.B., Nieto, F., Gutiérrez-Alonso, G., Walsh, E., 2011. Distinction Between Deformation and Contact Metamorphism by Very Low-Grade Metamorphism Indicators in the Georgeville Group (Nova Scotia, Canada), in: The Interrelationship Between Deformation and Metamorphism, University of Granada. pp. 38–39.

Agemar, T., Wörner, G., Heumann, A., 1999. Stable isotopes and amphibole chemistry on hydrothermally altered granitoids in the North Chilean Precordillera: A limited role for meteoric water? Contributions to Mineralogy and Petrology 136, 331–344. https://doi.org/10.1007/s004100050542

Anderson, J.L., Smith, D.R., 1995. The effects of temperature and fO2 on the Al-in-hornblende barometer. American Mineralogist 80, 549–559. https://doi.org/10.2138/am-1995-5-614

Atherton, M.P., Ghani, A.A., 2002. Slab breakoff: A model for Caledonian, Late Granite syn-collisional magmatism in the orthotectonic (metamorphic) zone of Scotland and Donegal, Ireland. Lithos 62, 65–85. https://doi.org/10.1016/S0024-4937(02)00111-1

Bea, F., Montero, P., Molina, J.F., 1999. Mafic Precursors, Peraluminous Granitoids, and Late Lamprophyres in the Avila Batholith: A Model for the Generation of Variscan Batholiths in

583 Iberia. The Journal of Geology 107, 399–419. https://doi.org/10.1086/314356
584 Bindeman, I., 2008. Oxygen Isotopes in Mantle and Crustal Magmas as Revealed by Single
585 Crystal Analysis. Reviews in Mineralogy and Geochemistry 69, 445–478.
586 https://doi.org/10.2138/rmg.2008.69.12
587 Boroughs, S., Wolff, J.A., Ellis, B.S., Bonnichsen, B., Larson, P.B., 2012. Evaluation of models
588 for the origin of Miocene low-δ18O rhyolites of the Yellowstone/Columbia River Large
589 Igneous Province. Earth and Planetary Science Letters 313–314, 45–55.
590 https://doi.org/10.1016/j.epsl.2011.10.039
591 Bowes, D.R., McArthur, A.C., 1976. Nature and Genesis of the Appinite Suite. Krystalinikum
592 12, 31–46.
593 Bucholz, C.E., Jagoutz, O., Vantongeren, J.A., Setera, J., Wang, Z., 2017. Oxygen isotope
594 trajectories of crystallizing melts: Insights from modeling and the plutonic record.
595 Geochimica et Cosmochimica Acta 207, 154–184.
596 https://doi.org/10.1016/j.gca.2017.03.027
597 Castro, A., Corretgé, L.G., Rosa, J.D.D.L.R., Fernández, C., López, S., García-Moreno, O.,
598 Chacón, H., 2003. The Appinite-Migmatite Complex of Sanabria, NW Iberian Massif,
599 Spain. Journal of Petrology 44, 1309–1344. https://doi.org/10.1093/petrology/44.7.1309
600 Chacko, T., Cole, D.R., Horita, J., 2001. Equilibrium Oxygen, Hydrogen and Carbon Isotope
601 Fractionation Factors Applicable to Geologic Systems. Reviews in Mineralogy and
602 Geochemistry 43, 1–81. https://doi.org/10.2138/gsrmg.43.1.1
603 Chazot, G., Lowry, D., Menzies, M., Mattey, D., 1997. Oxygen isotopic composition of hydrous
604 and anhydrous mantle peridotites. Geochimica et Cosmochimica Acta 61, 161–169.
605 https://doi.org/10.1016/S0016-7037(96)00314-6

606 Collins, W.J., Murphy, J.B., Johnson, T.E., Huang, H.Q., 2020. Critical role of water in the
607 formation of continental crust. Nature Geoscience 13, 331–338.
608 https://doi.org/10.1038/s41561-020-0573-6
609 Corgne, A., Schilling, M.E., Grégoire, M., Langlade, J., 2018. Experimental constraints on
610 metasomatism of mantle wedge peridotites by hybridized adakitic melts. Lithos 308–309,
611 213–226. https://doi.org/10.1016/j.lithos.2018.03.006
612 Demény, A., Casillas, R., Vennemann, T.W., Hegner, E., Nagy, G., Ahijado, A., De La Nuez, J.,
613 Sipos, P., Pilet, S., Milton, J., 2008. Plume-related stable isotope compositions and fluid–
614 rock interaction processes in the Basal Complex of La Palma, Canary Islands, Spain, in:
615 Coltori, M., Grégoire, M. (eds.), Metasomatism in Oceanic and Continental Lithospheric
616 Mantle. Geological Society, London, Special Publications, pp. 155–175.
617 https://doi.org/10.1144/SP293.8
618 Dobson, P.F., Epstein, S., Stolper, E.M., 1989. Hydrogen isotope fractionation between
619 coexisting vapor and silicate glasses and melts at low pressure. Geochimica et
620 Cosmochimica Acta 53, 2723–2730. https://doi.org/10.1016/0016-7037(89)90143-9
621 Donnelly, T., Waldron, S., Tait, A., Dougans, J., Bearhop, S., 2001. Hydrogen isotope analysis
622 of natural abundance and deuterium-enriched waters by reduction over chromium on-line to
623 a dynamic dual inlet isotope-ratio mass. Rapid communications in mass spectrometry 15,
624 1297–1303. https://doi.org/10.1002/rcm.361
625 Eiler, J.M., 2001. Oxygen Isotope Variations of Basaltic Lavas and Upper Mantle Rocks.
626 Reviews in Mineralogy and Geochemistry 43, 319–364.
627 https://doi.org/10.2138/gsrmg.43.1.319
628 Farver, J.R., 1989. Oxygen self-diffusion in diopside with application to cooling rate

629 determinations. Earth and Planetary Science Letters 92, 386–396.
630 https://doi.org/10.1016/0012-821X(89)90062-9
631 Feldstein, S.N., Lange, R.A., Vennemann, T., O'Neil, J.R., 1997. Ferric-ferrous ratios, H2O
632 contents and D/H ratios of phlogopite and biotite from lavas of different tectonic regimes.
633 Contributions to Mineralogy and Petrology 126, 51–66.
634 https://doi.org/10.1007/s004100050235
635 Fowler, M.B., 1988. Elemental evidence for crustal contamination of mantle-derived Caledonian
636 syenite by metasediment anatexis and magma mixing. Chemical Geology 69, 1–16.
637 https://doi.org/10.1016/0009-2541(88)90154-4
638 Fowler, M., Rollinson, H., 2012. Phanerozoic sanukitoids from Caledonian Scotland:
639 Implications for Archean subduction. Geology 40, 1079–1082.
640 https://doi.org/10.1130/G33371.1
641 Fowler, M.B., Henney, P.J., Darbyshire, D.P.F., Greenwood, P.B., 2001. Petrogenesis of high
642 Ba–Sr granites: the Rogart pluton, Sutherland. Journal of the Geological Society 158, 521–
643 534. https://doi.org/10.1144/jgs.158.3.521
644 Graham, C.M., Harmon, R.S., Sheppard, S.M.F., 1984. Experimental hydrogen isotope studies:
645 hydrogen isotope exchange between amphibole and water. American Mineralogist 69, 128–
646 138.
647 Hibbard, J.P., Staal, C.R. V, Rankin, D.W., 2007. A comparative analysis of pre-Silurian crustal
648 building blocks of the northern and and the southern Appalachian orogen. American Journal
649 of Science 307, 23–45. https://doi.org/10.2475/01.2007.02
650 Hoefs, J., 2018. Stable Isotope Geochemistry, 8th ed. Springer International Publishing AG.
651 Johnston, S.T., Thorkelson, D.J., 1997. Cocos–Nazca slab window beneath Central America.

652 Earth and Planetary Science Letters 146, 465–474. https://doi.org/10.1016/S0012-
653 821X(96)00242-7
654 Keppie, J.D., Dallmeyer, R.D., Murphy, J.B., 1990. Tectonic implications of 40 Ar/39 Ar
655 hornblende ages from late Proterozoic-Cambrian plutons in the Avalon Composite Terrane,
656 Nova Scotia, Canada. Geological Society of America Bulletin 102, 516–528.
657 https://doi.org/10.1130/0016-7606(1990)102%3C0516:TIOAAH%3E2.3.CO;2
658 Keppie, J.D., Davis, D.W., Krogh, T.E., 1998. U-Pb geochronological constraints on
659 Precambrian stratified units in the Avalon Composite Terrane of Nova Scotia, Canada:
660 tectonic implications. Canadian Journal of Earth Sciences 35, 222–236.
661 https://doi.org/10.1139/e97-109
662 Keppie, J.D., Dostal, J., Murphy, J.B., Nance, R.D., 1996. Terrane transfer between eastern
663 Laurentia and western Gondwana in the early Paleozoic: Constraints on global
664 reconstructions, in: Nance, R.D., Thompson, M.D. (eds.), Avalonian and Related Peri-
665 Gondwanan Terranes of the Circum North Atlantic. Geological Society of America Special
666 Paper 304, pp. 369–380. https://doi.org/10.1130/0-8137-2304-3.369
667 Kuroda, Y., Hariya, Y., Suzuoki, T., Matsuo, S., 1982. D/H fractionation between water and the
668 melts of quartz, K-feldspar, albite and anorthite at high temperature and pressure.
669 Geochemical Journal 16, 73–78. https://doi.org/10.2343/geochemj.16.73
670 Kyser, T.K., 1986. Stable isotope variations in the mantle, in: Valley, J.W., Taylor, H.P., O'Neil,
671 J.R. (eds.), Stable Isotopes. Reviews in Mineralogy and Geochemistry, pp. 141–162.
672 Kyser, T.K., O'Neil, J.R., 1984. Hydrogen isotope systematics of submarine basalts. Geochimica
673 et Cosmochimica Acta 48, 2123–2133. https://doi.org/10.1016/0016-7037(84)90392-2
674 Leake, B.E., Woolley, A.R., Birch, W.D., Burke, E.A.J., Ferraris, G., Grice, J.D., Hawthorne,

675 F.C., Kisch, H.J., Krivovichev, V.G., Schumacher, J.C., Stephenson, N.C.N., Whittaker,
676 E.J.W., 2004. Nomenclature of amphiboles: Additions and revisions to the International
677 Mineralogical Association's amphibole nomenclature. American Mineralogist 89, 883–887.
678 https://doi.org/10.1180/0026461046810182
679 Marks, M., Vennemann, T., Siebel, W., Markl, G., 2004. Nd-, O-, and H-isotopic evidence for
680 complex, closed-system fluid evolution of the peralkaline Ilímaussaq intrusion, south
681 Greenland. Geochimica et Cosmochimica Acta 68, 3379–3395.
682 https://doi.org/10.1016/j.gca.2003.12.008
683 Mathez, E.A., 1984. Influence of degassing on oxidation states of basaltic magmas. Nature 310,
684 371–375. https://doi.org/10.1038/310371a0
685 Moore, G., Carmichael, I.S.E., 1998. The hydrous phase equilibria (to 3 kbar) of an andesite and
686 basaltic andesite from western Mexico: constraints on water content and conditions of
687 phenocryst growth. Contributions to Mineralogy and Petrology 130, 304–319.
688 https://doi.org/10.1007/s004100050367
689 Müntener, O., Kelemen, P.B., Grove, T.L., 2001. The role of H2O during crystallization of
690 primitive arc magmas under uppermost mantle conditions and genesis of igneous
691 pyroxenites: an experimental study. Contributions to Mineralogy and Petrology 141, 643–
692 658. https://doi.org/10.1007/s004100100266
693 Murphy, J.B., 2013. Appinite suites: A record of the role of water in the genesis, Transport,
694 Emplacement and crystallization of magma. Earth-Science Reviews 119, 35–59.
695 https://doi.org/10.1016/j.earscirev.2013.02.002
696 Murphy, J.B., 2020. Appinite suites and their genetic relationship with coeval voluminous
697 granitoid batholiths. International Geology Review 62, 1–31.

https://doi.org/10.1080/00206814.2019.1630859

Murphy, J.B., Dostal, J., 2007. Continental mafic magmatism of different ages in the same terrane: Constraints on the evolution of an enriched mantle source. Geology 35, 335–338. https://doi.org/10.1130/G23072A.1

Murphy, J.B., Hynes, A.J., 1990. Tectonic control on the origin and orientation of igneous layering: An example from the Greendale Complex, Antigonish Highlands, Nova Scotia, Canada. Geology 18, 403–406. https://doi.org/10.1130/0091-7613(1990)018<0403:TCOTOA>2.3.CO;2

Murphy, J.B., Blais, S.A., Tubrett, M., McNeil, D., Middleton, M., 2012. Microchemistry of amphiboles near the roof of a mafic magma chamber: Insights into high level melt evolution. Lithos 148, 162–175. https://doi.org/10.1016/j.lithos.2012.06.012

Murphy, J.B., Keppie, J.D., Davis, D., Krogh, T.E., 1997a. Regional significance of new U-Pb age data for Neoproterozoic igneous units in Avalonian rocks of northern mainland Nova Scotia, Canada. Geological Magazine 134, 113–120. https://doi.org/10.1017/S0016756897006596

Murphy, J.B., Hynes, A.J., Cousens, B., 1997b. Tectonic influence on Late Proterozoic Avalonian magmatism: An example from the Greendale complex, Antigonish Highlands, Nova Scotia, Canada, in: Sinha, A.K., Whalen, J.B., Hogan, J.P. (eds.), Geological Survey of America Memoir 191. pp. 255–274. https://doi.org/10.1130/0-8137-1191-6.255

Murphy, J.B., Keppie, J.D., Dostal, J., Hynes, A.J., 1990. Late Precambrian Georgeville group: a volcanic arc rift succession in the Avalon Terrane of Nova Scotia. Geological Society London, Special Publication 51, 383–393. https://doi.org/10.1144/GSL.SP.1990.051.01.25

Murphy, J.B., Nance, R.D., 1989. Model for the evolution of the Avalonian-Cadomian belt.

721 Geology 17, 735–738. https://doi.org/10.1130/0091-
722 7613(1989)017<0735:MFTEOT>2.3.CO;2
723 Nance, R.D., Murphy, J.B., 1994. Contrasting basement isotopic signatures and the palinspastic
724 restoration of peripheral orogens: Example from the Neoproterozoic Avalonian-Cadomia
725 belt. Geology 22, 617–620. https://doi.org/10.1130/0091-
726 7613(1994)022<0617:CBISAT>2.3.CO;2
727 Nance, R.D., Murphy, J.B., 1996. Basement isotopic signatures and Neoproterozoic
728 paleogeography of Avalonian-Cadomiam and related terranes in the circum-North Atlantic,
729 in: Nance, R.D., Thompson, M.D. (eds.), Avalonian and Related Peri-Gondwanan Terranes
730 of the Circum North Atlantic. Geological Society of America Special Paper 304, pp. 333–
731 346.
732 Pál-Molnár, E., Batki, A., Kiss, B., Upton, B.G.J., Markl, G., Odling, N., Harangi, S., 2015.
733 Origin of mafic and ultramafic cumulates from the Ditrău Alkaline Massif, Romania. Lithos
734 239, 1–18. https://doi.org/10.1016/j.lithos.2015.09.022
735 Pe-Piper, G., Piper, D.J.W., 2018. The Jeffers Brook diorite–granodiorite pluton: style of
736 emplacement and role of volatiles at various crustal levels in Avalonian appinites, Canadian
737 Appalachians. International Journal of Earth Sciences 107, 863–883.
738 https://doi.org/10.1007/s00531-017-1536-z
739 Pearce, J.A., 1983. Role of the Sub-continental Lithosphere in Magma Genesis at Active
740 Continental Margins, in: Hawkesworth, C.J., Norry, M.. (eds.), Continental Basalts and
741 Mantle Xenoliths. Shiva Publications, Nantwich, Cheshire, pp. 230–249.
742 Pitcher, W.S., 1997. The Nature and Origin of Granite, 2nd ed. Chapman and Hall, London.
743 Pitcher, W.S., Berger, A.R., 1972. The Appinite suite: basic rocks genetically associated with

granite, in: The Geology of Donegal. A Study of Granite Emplacement and Unroofing. Regional Geology Series. John Wiley and Sons Ltd, Chichester, Sussex, pp. 143–168.

Pitcher, W.S., Hutton, D.H.W., 2003. A Master Class Guide to the Granites of Donegal: Geological Survey of Ireland. Geological Survey of Ireland.

Putirka, K., 2016. Amphibole thermometers and barometers for igneous systems and some implications for eruption mechanisms of felsic magmas at arc volcanoes. American Mineralogist 101, 841–858. https://doi.org/10.2138/am-2016-5506

Ridolfi, F., Renzulli, A., 2012. Calcic amphiboles in calc-alkaline and alkaline magmas: thermobarometric and chemometric empirical equations valid up to 1,130 °C and 2.2 GPa. Contributions to Mineralogy and Petrology 163, 877–895. https://doi.org/10.1007/s00410-011-0704-6

Rock, N.M.S., 1990. Lamprophyres. Blackie, Glasgow.

Sato, M., 1978. Oxygen fugacity of basaltic magmas and the role of gas-forming elements. Geophysical Research Letters 5, 447–449. https://doi.org/10.1029/GL005i006p00447

Sharp, Z.D., 1990. A laser-based microanalytical method for the in situ determination of oxygen isotope ratios of silicates and oxides. Geochimica et Cosmochimica Acta 54, 1353–1357. https://doi.org/10.1016/0016-7037(90)90160-M

Shaw, A.M., Hauri, E.H., Behn, M.D., Hilton, D.R., Macpherson, C.G., Sinton, J.M., 2012. Long-term preservation of slab signatures in the mantle inferred from hydrogen isotopes. Nature Geoscience 5, 224–228. https://doi.org/10.1038/ngeo1406

Shaw, A.M., Hauri, E.H., Fischer, T.P., Hilton, D.R., Kelley, K.A., 2008. Hydrogen isotopes in Mariana arc melt inclusions: Implications for subduction dehydration and the deep-Earth water cycle. Earth and Planetary Science Letters 275, 138–145.

https://doi.org/10.1016/j.epsl.2008.08.015

Sheppard, S.M.F., 1986a. Characterization and isotopic variations in natural waters, in: Valley, J.W., Taylor, H.P., O'Neil, J.R. (eds.), Stable Isotopes. Reviews in Mineralogy and Geochemistry, pp. 165–181.

Sheppard, S.M.F., 1986b. Igneous rocks; III, Isotopic case studies of magmatism in Africa, Eurasia and oceanic islands, in: Valley, J.W., Taylor, H.P., O'Neil, J.R. (eds.), Stable Isotopes. Reviews in Mineralogy and Geochemistry, pp. 319–371.

Sisson, Virginia B, Pavlis, Terry L, Roeske, Sarah M, Thorkelson, D.J., 2003. Introduction: An overview of ridge-trench interactions in modern and ancient settings, in: Sisson, V.B., Roeske, S.M., Pavlis, T.L. (eds.), Geology of a Transpressional Orogen Developed during Ridge-Trench Interaction along the North Pacific Margin. Geological Society of America Special Paper, Boulder, Colorado, pp. 1–18. https://doi.org/10.1130/0-8137-2371-X.1

Sun, S.S., McDonough, W.F., 1989. Chemical and isotopic systematics of oceanic basalts: Implications for mantle composition and processes, in: Saunders, A.D., Norry, M.J. (eds.), Magmatism in the Ocean Basins. Geological Society Special Publication, pp. 313–345. https://doi.org/10.1144/GSL.SP.1989.042.01.19

Suzuoki, T., Epstein, S., 1976. Hydrogen isotope fractionation between OH-bearing minerals and water. Geochimica et Cosmochimica Acta 40, 1229–1240. https://doi.org/10.1016/0016-7037(76)90158-7

Taylor, B.E., Eichelberger, J.C., Westrich, H.R., 1983. Hydrogen isotopic evidence of rhyolitic magma degassing during shallow intrusion and eruption. Nature 306, 541–545. https://doi.org/10.1038/306541a0

Taylor, H.P., 1968. The Oxygen Isotope Geochemistry of Igneous Rocks. Contributions to

790 Mineralogy and Petrology 19, 1–71. https://doi.org/10.1007/BF00371729
791 Tiepolo, M., Tribuzio, R., Langone, A., 2011. High-Mg andesite petrogenesis by amphibole
792 crystallization and ultramafic crust assimilation: Evidence from Adamello hornblendites
793 (Central Alps, Italy). Journal of Petrology 52, 1011–1045.
794 https://doi.org/10.1093/petrology/egr016
795 Ulrych, J., Krmíček, L., Teschner, C., Skála, R., Adamovič, J., Ďurišová, J., Křížová, Š.,
796 Kuboušková, S., Radoň, M., 2018. Chemistry and Sr-Nd isotope signature of amphiboles of
797 the magnesio-hastingsite–pargasite–kaersutite series in Cenozoic volcanic rocks: Insight
798 into lithospheric mantle beneath the Bohemian Massif. Lithos 312–313, 308–321.
799 https://doi.org/10.1016/j.lithos.2018.05.017
800 Valley, J.W., 2003. Oxygen Isotopes in Zircon. Reviews in Mineralogy and Geochemistry 53,
801 343–385. https://doi.org/10.2113/0530343
802 Valley, J.W., Kinny, P.D., Schulze, D.J., Spicuzza, M.J., 1998. Zircon megacrysts from
803 kimberlite: oxygen isotope variability among mantle melts. Contributions to Mineralogy
804 and Petrology 133, 1–11. https://doi.org/10.1007/s004100050432
805 Valley, J.W., Lackey, J.S., Cavosie, A.J., Clechenko, C.C., Spicuzza, M.J., Basei, M.A.S.,
806 Bindeman, I.N., Ferreira, V.P., Sial, A.N., King, E.M., Peck, W.H., Sinha, A.K., Wei, C.S.,
807 2005. 4.4 billion years of crustal maturation: Oxygen isotope ratios of magmatic zircon.
808 Contributions to Mineralogy and Petrology 150, 561–580. https://doi.org/10.1007/s00410-
809 005-0025-8
810 Vennemann, T.W., O'Neil, J.R., 1996. Hydrogen isotope exchange reactions between hydrous
811 minerals and molecular hydrogen: I. A new approach for the determination of hydrogen
812 isotope fractionation at moderate temperatures. Geochimica et Cosmochimica Acta 60,

2437–2451. https://doi.org/10.1016/0016-7037(96)00103-2

White, C.E., Barr, S.M., Hamilton, M.A., Murphy, J.B., 2021. Age and tectonic setting of Neoproterozoic granitoid rocks, Antigonish Highlands, Nova Scotia, Canada: Implications for Avalonia in the northern Appalachian orogen. Canadian Journal of Earth Sciences 59. https://doi.org/https://doi.org/10.1139/cjes-2020-0110

Wilkin, R.T., Bornhorst, T.J., 1993. Archean appinites from the Northern Complex, Michigan. Journal of Geology 101, 107–114. https://doi.org/10.1086/648199

Wolff, J.A., Balsley, S.D., Gregory, R.T., 2002. Oxygen isotope disequilibrium between quartz and sanidine from the Bandelier Tuff, New Mexico, consistent with a short residence time of phenocrysts in rhyolitic magma. Journal of Volcanology and Geothermal Research. https://doi.org/10.1016/S0377-0273(02)00214-7

Ye, H.M., Li, X.H., Li, Z.X., Zhang, C.L., 2008. Age and origin of high Ba-Sr appinite-granites at the northwestern margin of the Tibet Plateau: Implications for early Paleozoic tectonic evolution of the Western Kunlun orogenic belt. Gondwana Research 13, 126–138. https://doi.org/10.1016/j.gr.2007.08.005

Zheng, Y.-F., 1993. Calculation of oxygen isotope fractionation in magmatic rocks. Chemical Geology 120, 247–263. https://doi.org/10.1016/0012-821X(93)90243-3

833 **Figure Captions**

834 Figure 1.

835 (a) Global reconstruction of Avalonia and Cadomia along the periphery of Gondwana (after
836 Keppie et al., 1996; Nance and Murphy, 1996, 1994) showing subduction along the length of
837 Avalonia and Cadomia with a transform fault. (b) Tectonic map of the northern Appalachian
838 orogen (from Murphy et al., 2012 after Hibbard et al., 2007) with inset showing northern
839 Antigonish Highlands, within the Avalon terrane (Avalonia) of Nova Scotia. CBI, Cape Breton
840 Island; NB, New Brunswick; NE, New England; NL, Newfoundland; NS, Nova Scotia; QUE,
841 Quebec. (c) Geological map of the northern Antigonish Highlands displaying the Greendale
842 Complex between the Hollow and Greendale faults, intruding late Neoproterozoic Georgeville
843 Group (from Murphy et al., 2012 after Murphy et al., 1997b). U-Pb data boxed (see text for
844 details).

845

846 Figure 2.

847 (a) Mixing and mingling of felsic, mafic and ultramafic appinite. Acicular hornblendes appear to
848 co-precipitate with plagioclase. (b) Ultramafic layer intruded by a conjugate set of felsic veins.
849 (c) Mafic porphyry displaying a “stacked log” linear fabric defined by amphibole oriented
850 perpendicular to vein walls. Felsic veins cross-cut this sequence. (d) Acicular hornblende crystals
851 in cross section displaying “salt and pepper” texture and co-precipitation with plagioclase.

852

853 Figure 3.

854 (a) Hornblende (Hbl) from an ultramafic rock with inclusions of olivine (Ol) and serpentine
855 (Srp), olivine has locally broken down to serpentine. (b) Ultramafic sample displaying poikilitic

hornblende enclosing olivine and clinopyroxene (Cpx). (c) Hornblende from an ultramafic sample showing mineral growth sequence with olivine enclosed by clinopyroxene which itself is enclosed by hornblende. (d) Hornblende from a mafic sample showing coprecipitation of hornblende and plagioclase (Pl). (e) Core of saussurite (Sst) with rim of fresh albite (Ab) in contact with hornblende in a mafic rock. (f) Hornblende from a felsic rock showing co-precipitation with plagioclase, extensive sericitisation of feldspathic matrix is visible.

Figure 4.

4-Fold Al apfu (Al^{IV}) plotted against Al total apfu (Al^{tot}) for amphiboles from mafic and ultramafic rocks (data from Murphy et al., 2012). Procedure for assigning Al according to Leake et al. (2004). Dashed line indicates composition of Edenite (Ed) and Tschermak (Ts) substitutions.

Figure 5.

Chondrite-normalized REE diagram for Group A and B amphiboles from ultramafic rocks (modified from Murphy et al. 2012). Chondrite normalized values from Sun and McDonough (1989).

Figure 6.

Histogram showing $\delta^{18}O$ values for amphiboles from ultramafic, mafic and felsic rocks. Interpreted Group B and Group A ranges are shown above the histogram using data for mantle zones from Valley et al. (1998), zircon 5.3 ± 0.6 ‰; Bindeman (2008), MORB 5.7 ± 0.2 ‰;

878 Chazot et al. (1997), amphibole 5.3–5.6 ‰, and associated supracrustal zones from Valley et al.
879 (2005), > 5.9 ‰. Group A range interpreted from Bindeman (2008).
880
881 Figure 7.
882 Histogram showing δD values for amphiboles from ultramafic, mafic and felsic rocks.
883
884 Figure 8.
885 (a) Fe_{tot} a.p.f.u. (atoms per formula unit; from Murphy et al., 2012) versus δD. No correlation
886 between these two parameters is visible. (b) Calculated Fe^{3+}/Fe^{2+} ratios (from Murphy et al.,
887 2012) versus δD values for amphiboles from mafic and ultramafic rocks. A weak inverse
888 correlation is visible.
889
890 Figure 9.
891 (a) Calculated δD_{fluid}-$\delta^{18}O_{fluid}$ plot of amphibole fluid source from ultramafic, mafic and felsic
892 rocks. Fields for organic, metamorphic and primary magmatic waters are from Sheppard
893 (1986a). δD_{fluid} is calculated using fractionation equation from Graham et al. (1984). $\delta^{18}O_{fluid}$ is
894 calculated using fractionation equation from Zheng (1993). Both calculations are made for a
895 temperature estimate of 700 °C. (b) Calculated δD_{fluid}-$\delta^{18}O_{fluid}$ plot of amphibole fluid source
896 from ultramafic, mafic and felsic rocks. Fields for organic, metamorphic and primary magmatic
897 waters are from Sheppard (1986a). δD_{fluid} is calculated using fractionation equation from
898 Suzuoki & Epstein (1976). $\delta^{18}O_{fluid}$ is calculated using fractionation equation from (Zheng,
899 1993). Both calculations are made for a temperature estimate of 700 °C.
900

Figure 10.

(a) 4-Fold Al apfu (Al^{IV}) plotted against Al total apfu (Al^{tot}) for amphiboles from mafic and ultramafic rocks (data from Murphy et al., 2012). Procedure for assigning Al according to Leake et al. (2004). Pressure estimates for 650 °C and 750 °C calculated using Anderson & Smith (1995). (b) Al_2O_3 (wt. % from Murphy et al., 2012) plotted against pressure estimates, technique from Pál-Molnár et al. (2015). Laser ablation sample sites listed on x-axis. PG4, PG12, PG6, PG11, PG1 refer to amphiboles from ultramafic rocks. GR8-M, GR15-M, GR10-M and GR9-M refer to amphiboles from mafic rocks samples.

Figure 11.

(a) Calculated δD_{fluid}-H_2O (wt. %) plot showing progressive hydration trend of amphiboles from ultramafic, mafic and felsic rocks. δD_{fluid} is calculated using fractionation equation from Graham et al. (1984) at 700 °C. (b) Calculated δD_{fluid}-H_2O (wt. %) plot showing progressive hydration trend of amphiboles from ultramafic, mafic and felsic rocks. δD_{fluid} is calculated using fractionation equation from Suzuoki & Epstein (1976) at 700 °C.

Figure 12.

Conceptual model showing the development of a slab window by ridge-trench interaction (modified from Murphy, 2020 after Sisson et al., 2003). Note location of Greendale Complex next to Hollow-Greendale fault and association with Antigonish Granites and other felsic magmas. Detail on right (modified from Murphy, 2020) shows progressive ascent of magma next to Hollow-Greendale fault. Symbols indicate throw on Hollow-Greendale fault system. 1) dissolved mantle water in magma system, 2) crystallization of Group B hornblende with mantle

derived fluids, 3) shallow crust crystallization of Group A hornblende with mixed water sources including assimilation of earlier hydrothermally altered phases. Progressive ascent of magma system results in re-equilibration of Group B hornblende following the assimilation of supracrustal sedimentary and volcanic rocks. Felsic magmas form by fractionation of a mafic parent, by anatexis (hydrous melting) of the lower crust as shown by Sm-Nd data from Murphy & Dostal (2007). They rise to the mid- and upper-crust and form a rheological barrier to the subsequent ascent of mafic magma. Early mafic intrusions are entrained as enclaves so that only the appinites at the extremities of the system are preserved intact.

Figures

Figure 1.

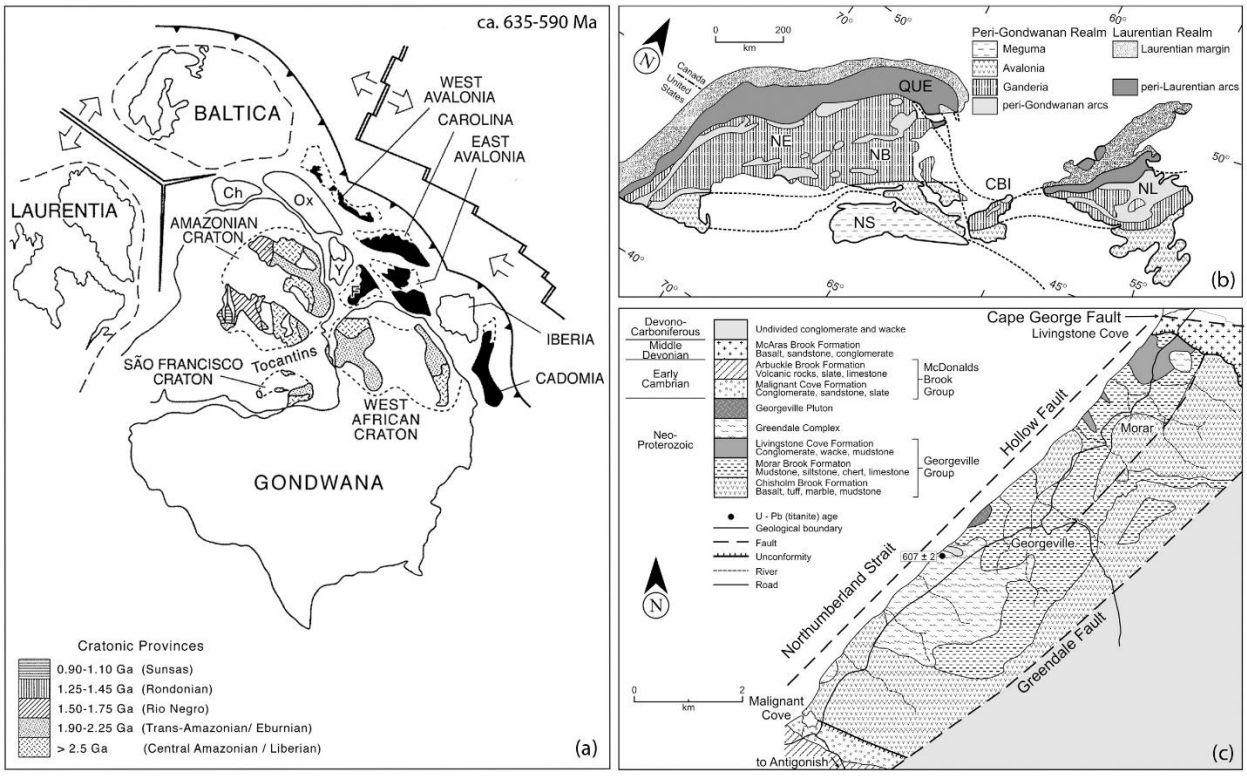

937 Figure 2.

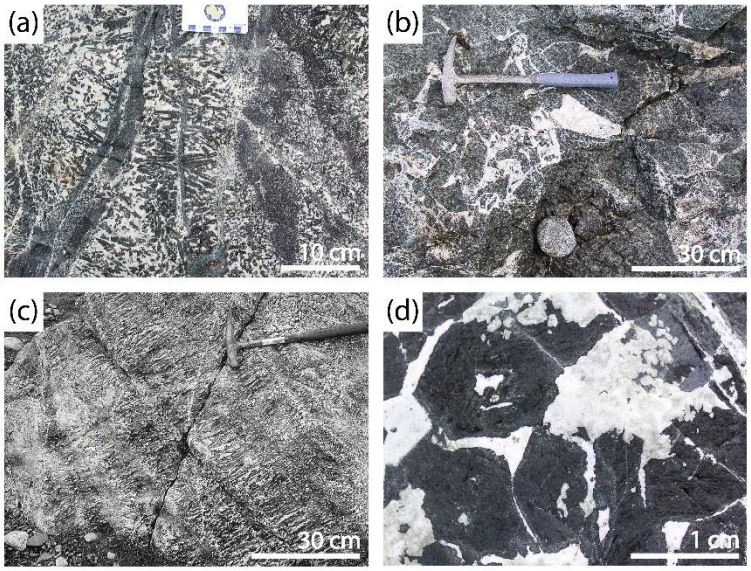

938

939 Figure 3.

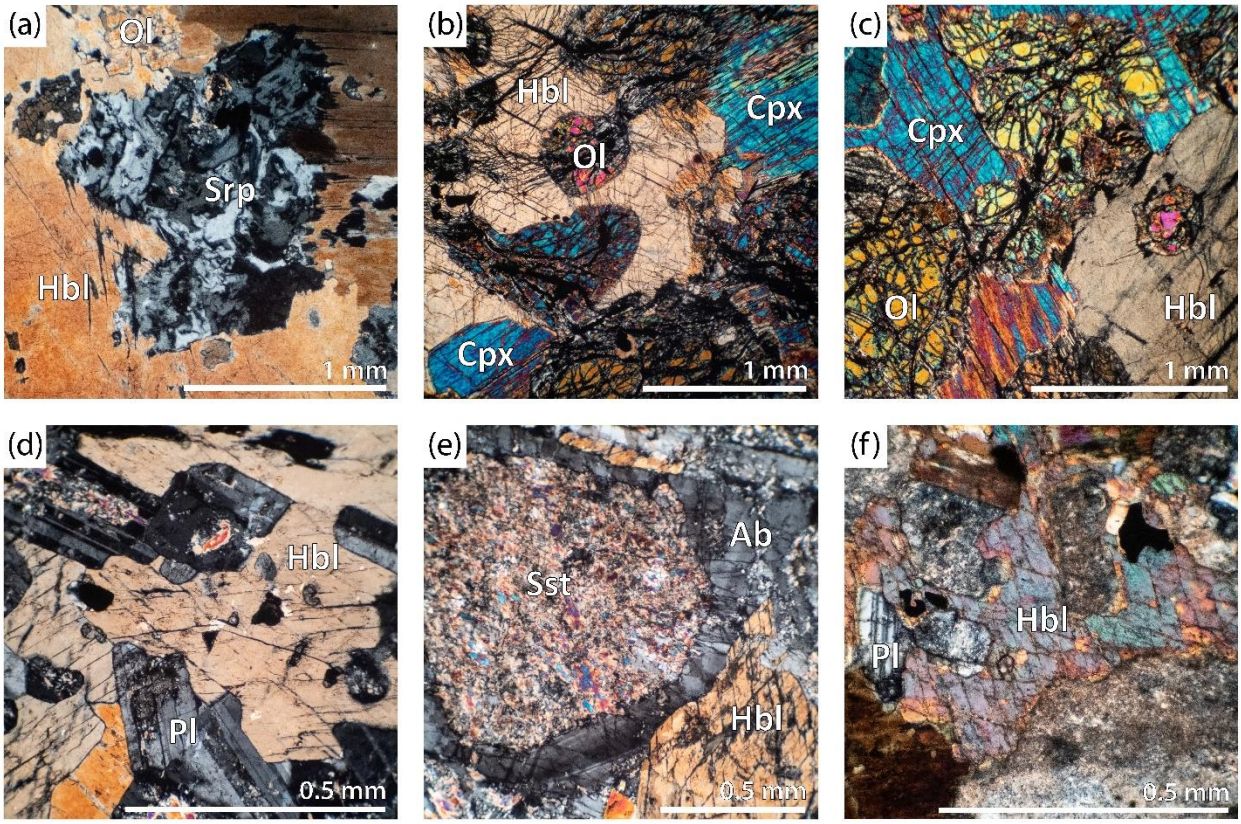

940

941

942 Figure 4.

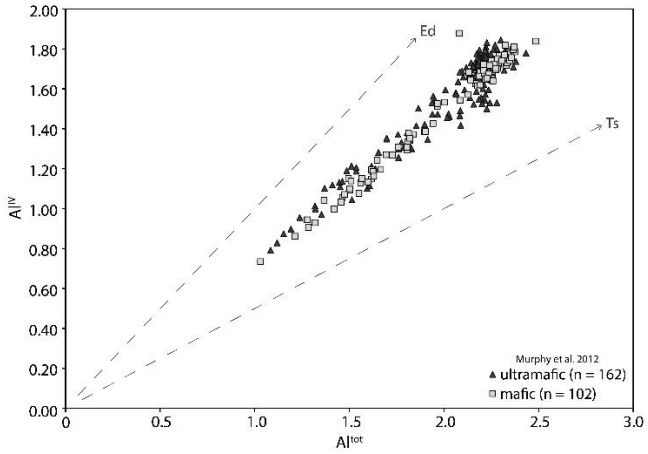

943

944

945 Figure 5.

946

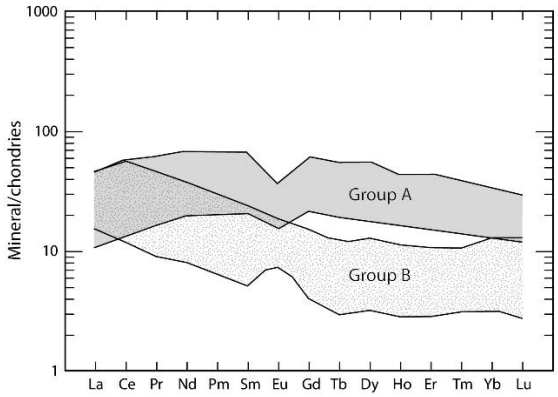

947

948 Figure 6.

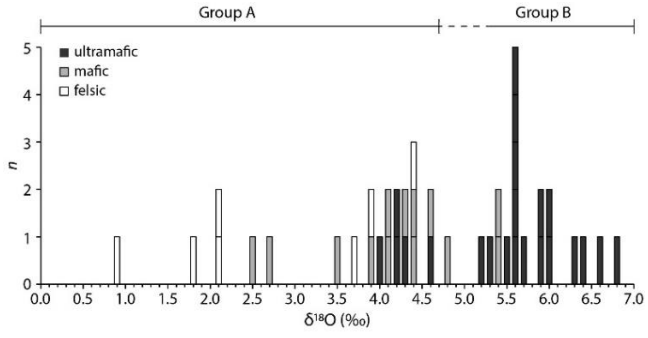

949

950

951 Figure 7.

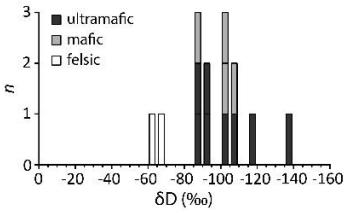

Figure 8.

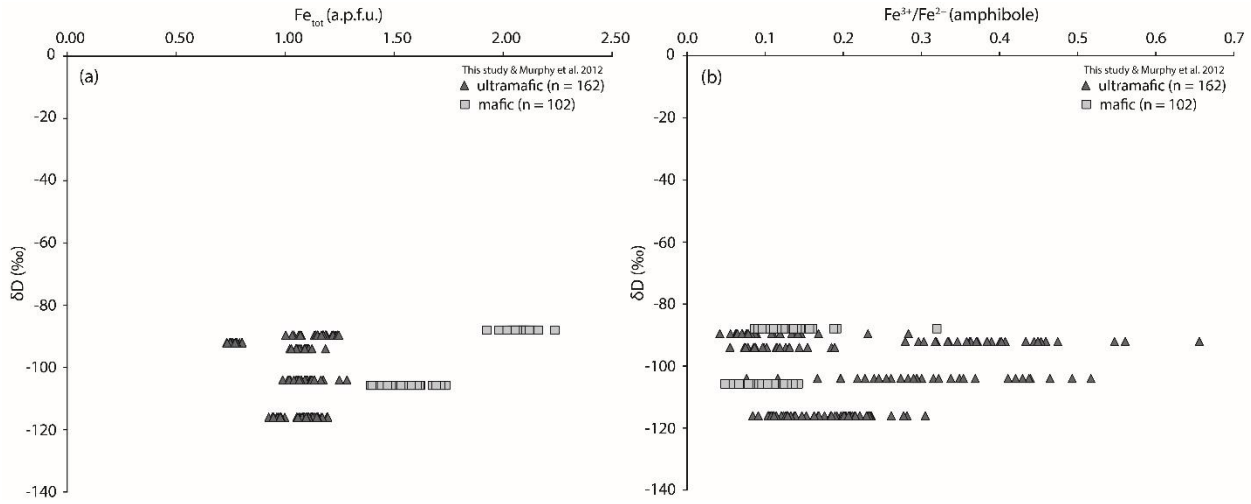

Figure 9.

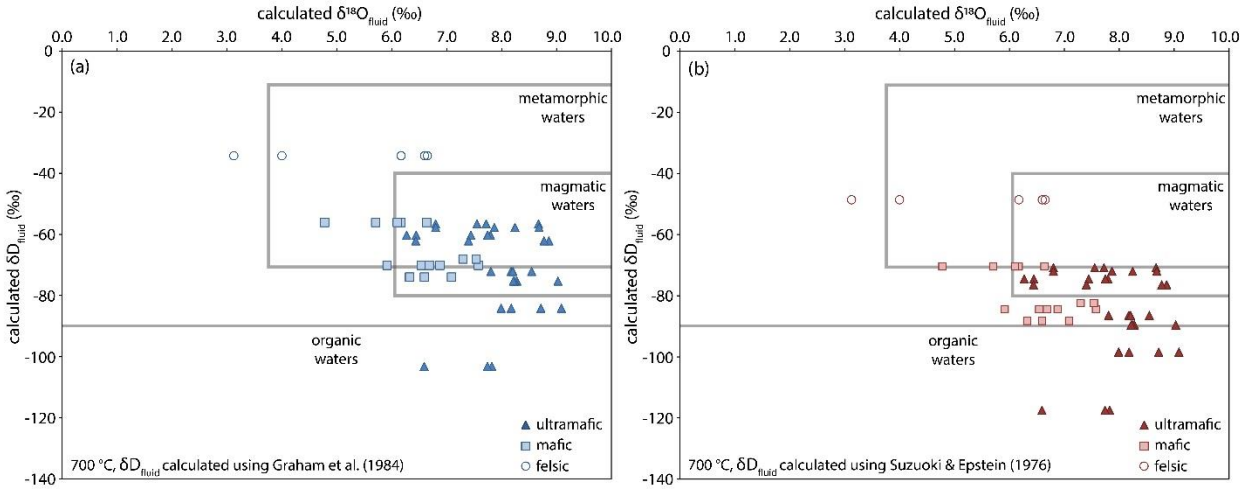

Figure 10.

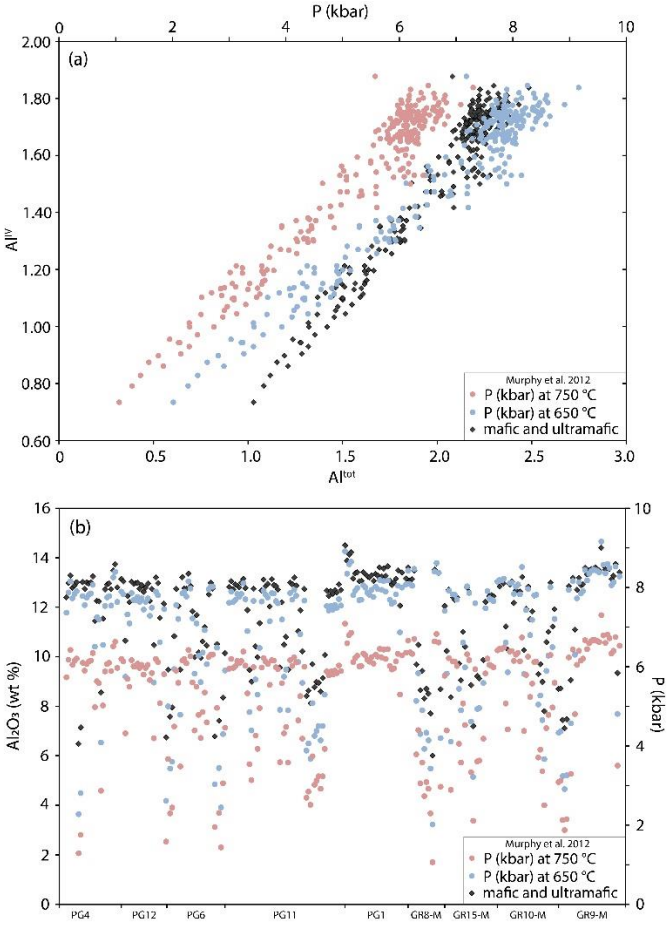

Figure 11.

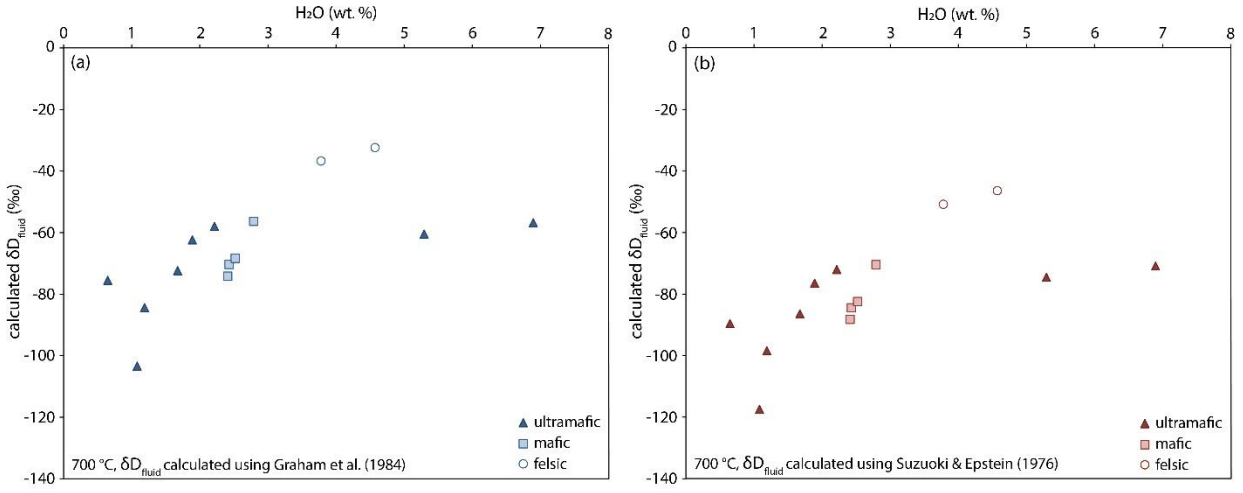

965

966 Figure 12.

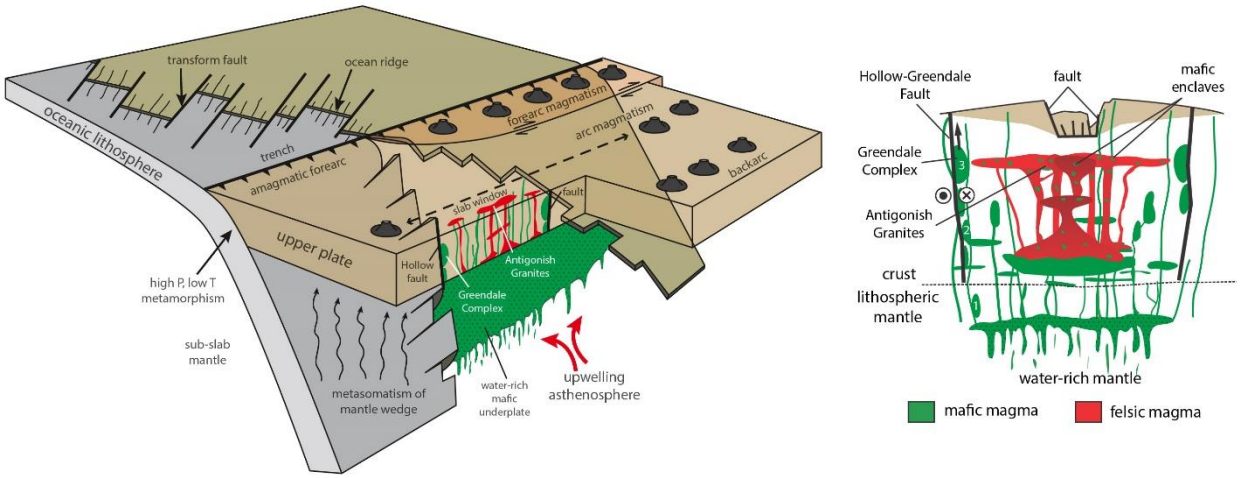

967

968

969

970 **Table captions**

971 Table 1. $\delta^{18}O$ of drilled amphibole and single mineral separates from Greendale Complex
972 litholigies (‰ V-SMOW). $\delta^{18}O$ water is calculated using the equations of Zheng (1993) at a
973 temperature average of 700 °C.

974

975 Table 2. δD of single mineral separates from Greendale Complex litholigies (‰ V-SMOW). δD
976 water[a] is calculated using the equations of Graham et al. (1984) and δD water[b] is calculated using
977 the equations of Suzuoki & Epstein (1976), both calculations use a temperature average of
978 700 °C.

Tables

Table 1

Sample	Unit	$\delta^{18}O$ amphibole (‰ V-SMOW)	$\delta^{18}O$ water (‰ V-SMOW) T 700 °C	Average $\delta^{18}O$ amphibole (‰ V-SMOW)	σ
PG1-A	ultramafic	4.2	6.4	4.9	0.7
PG1-B		5.6	7.8		
PG1-C		5.2	7.4		
PG1-D		5.5	7.8		
PG1-X		4.0	6.3		
PG2-A*	ultramafic	6.4	8.7	5.4	0.8
PG2-B*		5.5	7.7		
PG2-C*		5.3	7.6		
PG2-X*		4.6	6.8		
PG4-A	ultramafic	6.0	8.2	5.7	0.8
PG4-B		4.6	6.8		
PG4-C		5.6	7.9		
PG4-X		6.4	8.7		
PG5-A*	ultramafic	6.8	9.0	6.2	0.4
PG5-B*		6.0	8.3		
PG5-C*		6.0	8.2		
PG5-X*		6.0	8.2		
PG6-A	ultramafic	5.6	7.8	5.9	0.3
PG6-B		6.3	8.6		
PG6-C		5.9	8.2		
PG6-X		6.0	8.2		
PG7-A	ultramafic	5.6	7.8	5.3	0.7
PG7-B		4.3	6.6		
PG7-C		5.6	7.8		
PG7-X		5.5	7.7		
PG-11-A	ultramafic	5.9	8.2	6.2	0.5
PG11-C		6.8	9.1		
PG11-D*		6.5	8.7		
PG11-X		5.7	8.0		
PG12-A	ultramafic	4.2	6.4	5.6	1.2
PG12-B		6.6	8.9		
PG12-C		5.2	7.4		
PG12-X2*		6.5	8.8		
GR9-M-A	mafic	4.1	6.3	4.3	0.4
GR9-M-B		2.7	5.0		
GR9-M-C		4.4	6.6		
GR9-M-D		4.8	7.1		
GR9-M-E*		2.1	4.4		
GR9-M-X		4.1	6.3		
GR15-M-A	mafic	2.5	4.8	3.6	0.7
GR15-M-B		3.5	5.7		
GR15-M-D		3.9	6.2		
GR15M-E*		4.4	6.6		
GR15-M-X		3.9	6.1		
GX1-A	mafic	4.3	6.5	4.5	0.6
GX1-B		4.4	6.7		
GX1-C		4.6	6.9		
GX1-D		3.7	5.9		
GX1-X		5.3	7.6		
GX2-X	mafic	5.3	7.5	5.2	0.2
GX2-X2*		5.1	7.3		
GR8-F-A	felsic	2.1	4.4	2.1	
GR9-F-A	felsic	2.1	4.3	2.1	
GR5-F-A	felsic	0.9	3.1	3.1	1.6
GR5-F-B		1.8	4.0		
GR5-F-C		3.9	6.2		
GR5-F-E*		4.4	6.6		
GR5-F-X		4.4	6.7		

982 * Indicates use of second standard set (2019 samples) YP2, GP147 and UWG2. Labels without *

983 indicate initial sample set (2017 samples) using TOR1, YP2, SCXO, JJB8 and GP147 standards.

984

985 Table 2

Sample	Unit	δD amphibole (‰ V-SMOW)	δD water[a] (‰ V-SMOW) T 700 °C	δD water[b] (‰ V-SMOW) T 700 °C
PG1	ultramafic	-92	-60	-75
PG2	ultramafic	-88	-57	-71
PG4	ultramafic	-90	-58	-72
PG5	ultramafic	-107	-75	-90
PG6	ultramafic	-104	-72	-87
PG7	ultramafic	-135	-103	-118
PG11	ultramafic	-116	-84	-99
PG12	ultramafic	-94	-62	-77
GR9-M	mafic	-106	-74	-88
GR15-M	mafic	-88	-56	-71
GX1	mafic	-102	-70	-85
GX2	mafic	-100	-68	-82
GR5-F	felsic	-64	-32	-47
		-68	-37	-51

986